Application of Cylindrical Near-Field Measurement Technique To The Calibration Of Spaceborne Radar Antennas: NASA Scatterometer And SeaWinds

Ziad A. Hussein [1,2] and Yahya Rahmat-Samii [2]

'Jet Propulsion Laboratory
California Institute of Technology
Pasadena, Ca 91109

[2] University of California Los Angeles
Department of Electrical Engineering
Los Angeles, California 90024-1594

Submitted to IEEE Geoscience and Remote Sensing Transaction

Abstract

Modern spaceborne radar scatterometers such as the NASA Scatterometer (NSCAT) and SeaWinds radar instruments require precise determination of the normalized backscattered radar cross section within a few tenth of a decibel in order to achieve the desired wind velocity and direction measurement accuracy of 2 m/s and 20 degrees respectively. This high level of precision requires a priori pre- launch accurate knowledge and determination of the radar antenna's absolute gain and relative radiation patterns characteristics over wide angular range. Such characterizations may be performed on a far-field range or in an indoor near-field measurement facility. Among the unique advantage of the latter is that many information of the radar antenna radiation properties can be obtained anywhere outside the near-field measurement surface. Two different recently designed radar scatterometers are considered in this paper, NASA Scatterometer (NSCAT) and SeaWinds, to demonstrate the utility of a newly completed cylindrical near-field measurement range for the calibration of spaceborne antennas. As an example of an advanced calibration methodology, the data based on a recently measured JPL/NASA scatterometer (NSCAT) radar antenna are used to experimentally demonstrate the role of the probe pattern compensation, probe multiple reflection effects, probe mis-positioning effects, scan area truncation effects, etc. A measurement test on a standard gain horn have been performed to achieve and verify the absolute gain calibration accuracy. A comparison between direct far-field measured data and those obtained from cylindrical near-field measurements for the SeaWinds radar antenna was found in excellent agreement.

1. INTRODUCTION

The evolution of spaceborne scatterometers is demanding very high quality performance from antennas. For example, a recently designed JPL/NASA scatterometer (NSCAT) instrument [1] for global mapping of dynamic change of ocean circulation requires very accurate knowledge of antenna gain, wide-angle antenna patterns, squint angle, and beamwidth. The antennas assembled on this instrument are each a ku-band 3-m long stick slotted waveguide type. Fig. 1 Shows the dual polarization H and V-pol NSCAT flight antenna. The use of an outdoor far field range is not suitable to calibrate this class of radar antennas in part because of the variable weather and the difficulty in obtaining accurate absolute gain and fine resolution three - dimensional radiation patterns over wide angular range for off boresight pointed beams. Given the size of the NSCAT antenna for an example, at 13.995 GHz, the far-field is beyond 800 meter and hence a proper antenna range, and antenna alignment must be used over that distance to carry such measurement.

An alternative approach to far-field radar antenna calibration is near-field indoor measurement [2]-[3]. Near field measurement may be performed in various configuration; however, this paper will focus on the cylindrical near field configuration. Once near-field data is acquired on a cylindrical surface surrounding the antenna as shown in Fig. 2, a data processing algorithm is used to give more details information on antenna radiation properties which would have required much conventional measurement work [4]-[8]. The antenna radiated fields - amplitude and phase- can be obtained anywhere outside the scanning cylindrical near-field surface. Besides this unique advantage, near-field measurement techniques is performed in a controlled environment - in an indoor shielded anecheoic chamber. Therefore, measurement can be carried out without disruption of weather conditions (rain, snow, ..etc.), unwanted signals, and to a high degree of room temperature control. Hence, near-field measurement eliminates the need for long test ranges, and in several respect with better measurement accuracy than conventional far-field measurement.

In order to accurately measure the radiation properties of these spaceborne scatterometers, a cylindrical near-field measurement facility has recently been developed at JPL [9]-[1 O] as shown in Fig. 3 It is well-known that special attention must be given to different near-field errors that might be present in the measurement in order to accurately characterize the wide-angle test antenna's patterns and gain [9],[10],[1 5]. One of the objectives of this paper is to present a calibration methodology to determine the effect of different near-field measurement errors including the sampling probe radiation properties on the test antenna absolute gain and patterns, and to critically assess the effect of these errors on the achievable accuracy in absolute gain and pattern measurement. In addition, the paper will demonstrate the application of the cylindrical near-field measurement technique, and a comprehensive calibration methodology to the measurement of large spaceborne scatterometers that have been recently calibrated at JPL.

This is done by presenting a simulation methodology for proper characterization of the probe pattern effects on the antenna far-field patterns [8]. **Using an analytically** well-**characterized probe with circular aperture, we have been able to examine the effects of** the probe. In particular, we have been able to carefully evaluate the role of the probe pattern and gain compensation in determining the far-field patterns of the test antenna (see Appendix A). Additionally, other sources of errors such as probe interaction with the antenna, mis-positioning of the probe, scan area truncation, receiver non-linearity and drift are evaluated to determine the achievable accuracy in the calibration of these antennas.

The paper is organized as follows. Section 2 presents an overview of the calibration methodology of scatterometer radar antennas, and discusses and presents the unique features of the cylindrical near-field calibration setup and measurement at JPL. Section 3 demonstrates the utility of cylindrical near-field measurement to calibrate ku-band sactterometer antenas, and presents a generalized algorithm in which to determine the effect of near-field errors on the predicted far-field patterns with specific application to

NSCAT. Section 4 discusses the calibration of another class of scatterometer radar antennas, SeaWinds, and verification methodology using ku-band standard gain horn. For completeness, a comparison between direct far-field measurement and those obtained from cylindrical near-field measurement are also presented. Summary of the paper is given in section 5.

2. CYLINDRICAL NEAR-FIELD MEASUREMENT: AN OVERVIEW

A. General Description

The theoretical basis of cylindrical near-field measurement is the application of the surface equivalence theorem. In general, the knowledge of the tangential fields (amplitude and phase) on a surface completely enclosing the test antenna enables the computation of the field anywhere in the region exterior to it. The exterior region in which antenna radiation properties can be obtained spans the near, fresnel, and far-field domain of the test antenna. Ordinarly, the measurement surfaces that can be easily realized in **practice are the planar surface in front of the antenna [16]-[1 9], a circular cylindrical** surface surrounding the antenna [4]-[9], and spherical surface that enclosing it [20]. Besides that these surfaces are mechanically convenient scanning surfaces, there is a unique mathematical advantage of carrying the near-field measurement in any of the **above coordinate system. This is simply put that the vector wave equations in these coordinates system are separable [16].**

Depending on the test antenna geometry a particular scanning surface is selected. Though, measurement made on a spherical surface, surface that encloses the test antenna, are good to characterize completely any type of antennas, the cylindrical (as well as the planar) measurement geometry, shown in Fig. 2, is usually finite in extent - and suitable for characterization of directive antennas. The cylindrical scanning surface can be achieved by rotating the antenna under test in azimuth while a sampling probe detects the electric field as it travels along a tower in a linear motion to a predetermined

positions (see subsection 3.C) . Hence, practical measurement on cylindrical surface (also planar), surface that don't extend to infinity, may yield to truncation errors in the computation of the far field. The error magnitude depends on the relative power level not measured outside the scanning area.

As an illustration, NSCAT antenna, shown in Fig. 1, posses a rectangular aperture with long length and narrow width. The relative near field power pattern for such an aperture is uniform along its aperture's length and tapered rapidly outside it. On the other hand, the aperture has a wide beam in the azimuth direction -along its narrow width- and the relative power pattern varies and tapered slowly in that direction. A scanning cylindrical geometry is then suitable to test this class of antennas. Since - for the case that the antenna is mounted in the vertical direction with the cylinder geometry concentric ring completely surrounding its narrower dimension-, the antenna doesn't radiate appreciably in the +/- z direction, and most of the radiating energy is captured by the cylindrical surface. Consequently, a very small truncation error may appear at far- angle from the main beam peak in the computed far-field pattern.

B. Far-Field From Cylindrical Near-Field Measurement

The vector wave expansions of the electromagnetic field of both the sampling probe and the test antenna in cylindrical coordinate system, and the application of the reciprocity theorem between them yield to the representation of the electromagnetic field anywhere outside the measurement surface. The field representation is written in terms of the near-field probe vector output response and the radiation characteristics of the probe when used as a transmitter [4]-[8]. Therefore, a priori to cylindrical near-field measurement, the probe radiation properties must be known. Noteworthy, the measurement uncertainty determined in the characterization of the probe is associated with the achievable accuracy of the test antenna performance parameters. See Appendix A for an overview of the mathematical developments.

C. Calibration Methodology

There are two types of bias errors that have been identified in the cylindrical near-field calibration: Electrical and Mechanical. The electrical errors are dominated by the probe pattern effect and gain [8], [12], probe-antenna under test interaction, scan area truncation, receiver non-linearity and drift, The mechanical errors which may also introduce bias errors in the calculated far-field patterns are mainly probe position with respect to the center of rotation of the test antenna, probe orientation and overall alignment. Fig, 4 shows the algorithm flow diagram that we have implemented to estimate the effect of these errors and ultimately provide guidance in tuning the near-field range to reduce the measurement uncertainties. For an example, a simulation model of NSCAT antenna is implemented and different near-field simulated and measured errors are introduced to determine both the magnitude of these errors and how it manifest itself in the far-field. An error control table is then established to assess the overall calibration uncertainties.

D. Unique Feature Of JPL Cylindrical Range

In the cylindrical near-field measurement facility at JPL, the sampling probe travels a single linear motion while the test antenna rotates in azimuth direction to form a cylindrical geometry [9]-[10] as shown in Figs. 2 and 3. The test antenna is mounted on a pedestal that rotates in the azimuth direction. A sampling orthomode probe travels along a rail tower in a linear motion to a predetermined positions separated by a distance Az. The maximum extent of the tower or scanner is 3.8 meter long. For each complete antenna rotation and fixed probe position, the sampling linearly polarized orthomode probe acquired data on a concentric ring for a fixed $\Delta\phi$. Data on a portion of the ring, corresponding to the position in which the back of the antenna is facing the probe, are not sampled. This is implemented to allow the probe to travel during this interval to the next sampling position at a distance, Az.

The data collected on each sampling position on the ring represents the co- and cross polarized (amplitude and phase) electric field components that are induced simultaneously on each port of the orthomode probe. This feature is accomplished with the use of an RF switch that electronically alternates between the input ports of the probe. In order to maintain the relative ratio between the measured field components, the insertion loss difference, amplitude and phase, of the RF switch is determined. This difference is corrected at the front panel of the SA 1795 receiver. An alternative method to the use of an orthomode probe is to acquire the co-polarized component with an open ended rectangular waveguide probe. The probe is then rotated by a 90" to obtain the cross polarized field component, This approach is time consuming, in particular when the receiver is required to be stable over the time required for near-field scanning, which may be hours. Fig. 2 shows the coordinate system (r_o, $n\Delta\phi$,$m\Delta z$) for the measured data. The sampling upper bound are $\Delta\phi=\lambda/2r$ and $\Delta z=\lambda/2$, in which r is the smallest cylinder radius enclosing the test antenna and n and m are the number of sampling points in ϕ and z respectively.

The data acquisition is completely automated. The signal source, HP 8673G, sends cw signal at the operating frequency to the test antenna through an RF transmit circuitry as depicted in Fig. 5. The transmit circuitry consists of a generator, an amplifier, a low pass filter, a 20 dB coupler to provide a reference signal, a step attenuator, variable attenuator and a phase shifter for insertion loss measurement, an RF rotary joint to allow AUT rotation without flexing the RF cable, and the test antenna. A position controller that receives position data from a laser interferometer (not shown in the figure) controls the motor drives moving the sampling probe. And, it triggers the receiver to take measurements at a predetermined probe positions. The sampling probe receives the signal from which its coupled through an RF switch and local oscillator unit to the SA 1795 receiver. An HP computer that drives the SA receiver stores the electric field data. This system of measurement configuration has been used to calibrate the SeaWinds radar antennas. Similar configuration was implemented for the Calibration of NSCAT antennas with the exception that an HP 8530 receiver was used rather than the SA 1795.

3. **NSCAT ANTENNA MEASUREMENT** AND RANGE CALIBRATION

A. NSCATAntenna Description and Mission Requirements

The NASA scatterometer, NSCAT, is a Microwave instrument, was designed to measure wind speed and direction over the Earth's ocean. The data set collected by the instrument has been used by many different science disciplines to name few, the climate change researchers, operational weather forecasters, and commercial ship routing firms. The NSCAT antenna designed for the instrument is a dual-pol (vertical and horizontal polarization) fan-beam that provides ground resolution of 25 X 7 km. It is made up of two separate slotted waveguide array- fed-horns as shown in Fig. 1. The antenna is 3.06 meter long and 0.063 meter wide operating at Ku-band (13.995GHz); Antenna directivity is approximately 34 dB. The mission required an accurate determination of the antennas radiation properties. This include the antenna absolute gain, 3-D patterns, pointing, and beamwidths.

B. A Generalized Technique to Determine the Effect of Probe Pattern and its ***Application to NSCA T Antenna***

In order to assess the effect of probe pattern and gain on the computation of the far-field of the test antenna, we have considered an analytically well -characterized probe with circular aperture in our calibration methodology (see Appendix A). The purpose of this is to determine the effect, and the importance of introducing the probe radiation properties in the computation of test antenna patterns for a given size probe. We were able to determine the angular region at which probe correction is needed, and estimate the magnitude of the error in that regions in the calibration of spaceborne radar antennas, and consequently design a sampling probe with single choke horn to be used in the measurement.

A simulation model that resembles the actual NSCAT flight antenna is implemented to obtain near-field using circular-aperture probe with an arbitrary radius (see Appendix A). In order to generate NSCAT-synthetic near-field data, a method of moment computation was implemented for the case that resemble the actual NSCAT flight antenna and probe size selected to be used in the cylindrical near-field measurement. Hence, we have considered a probe radius of $a=0.5\lambda$. The idealized circular aperture probe output integral (Appendix A equation 3) is then evaluated for each probe position on the required sampling point on a cylindrical near-field surface enclosing the NSCAT antenna. In order to show the effect of probe the far-field is then calculated with and without probe pattern compensation and compared to the exact results. Here, the exact results are the direct far-field result of the method moment model of NSACT antenna. Fig. 6 shows a comparison between the calculated far-field pattern with and without probe pattern comparison and the exact solution. As can be seen that the need for probe pattern compensation is pronounced at an angle starting at 20 degrees from the peak, and it is evident from the figure that the magnitude of the error becomes **larger at far-angle from the peak when no probe pattern compensation is applied. Also, one can observe that no probe compensation is needed within +/- 10 degrees from the peak of the beam.** A **cylindrical near-field measurement** of NSCAT antenna with dual orthomode probe (9.57 dB gain port 1 and 9.56 dB port 2) supported these observations. It is worthwhile to note here that a larger probe size may not be useful, since multiple scattering between the antenna and the probe becomes very large. In addition, the uncertainty in the probe pattern measurement becomes significant at close angels from the peak.

C. Probe Gain and Insertion Loss Measurement Effect on NSCAT *Antenna Gain*

An insertion loss measurement approach is implemented in our cylindrical near-field range to determine the NSCAT antenna gain. The sampling probe in this approach is used as a standard gain. Thus, in addition to the need of the knowledge of the radiation properties of the probe a priori to cylindrical near-field measurement, the

probe gain becomes necessary. The sampling probe was calibrated at the National Institute of Standard and Technology (NIST) with +/- 0.1 dB accuracy using an extrapolation technique [21]. This bias error becomes part of the overall antenna gain measurement uncertainty.

Additionally, other bias error may occur in the insertion loss measurement procedure. During this approach, the insertion loss difference between the test antenna and the probe, normally taken at the peak of the near-field (normalization point) on the sampling cylindrical surface, is determined. This is done by recording the open loop co- and cross polarized field components at the normalization point. Referring to Fig. 5, the 11-foot RF cable is then disconnected from the test antenna and connected to the cable leading to the probe. A known attenuation is then added (-30 dB for the co-polarized insertion loss measurement) to the calibrated Variable attenuator depicted in Fig. 5. A closed circuit loop is then obtained with both the antenna and the probe not connected. The variable attenuator is then adjusted until the receiver reads the open loop field normalization point. The insertion loss, amplitude and phase, is then recorded. The **only bias error that may occur during this process involves disconnecting and connecting the RF cable. This bias error is due to RF leakage and cable stretching. The latter normally translates its bias error as phase error. Similar** procedure are repeated to determine the cross polarized insertion loss. The bias error over repeated insertion loss measurements was found to be within +/- 0.03 dB.

D. Truncation in Z

In principle, the integral in z in equation 16 (Appendix A) should extend to infinity. This is of course not possible, and hence we should determine what errors are introduced by using a finite scan in z. To determine the effect of the finite scan in z for good accuracy, data was taken over the maximum extent of the scanner 3.81 meter. The far-field is then computed with the use of the complete near-field data set obtained at r_o =33.6 inches. Next we truncate data points on both edge of the scan and we

compute the far-field. The differences in antenna gain are shown **in** Fig. 7 as a function of the truncated distance. It is evident from the curve in Fig. 7 that the scan length which is only slightly larger than the antenna is sufficient for good accuracy at the indicated r_0=33.6 inch separation distance. Also, it is evident that the truncated near-field regions corresponds mainly to the field diffracted around the edge of the antenna, where the near-field tapered rapidly on both sides outside the aperture of the antenna, contribute mainly to the wide-angle regions of the far-field sidelobe level and periodicity.

E. Truncation in ϕ

A portion of the azimuthal scan in ϕ (-30° < ϕ < 30°) degrees was not sampled. This is implemented to give the probe enough time to travel during this interval to a predetermined position Az. The angular region truncated is +/- 30 degrees. In order to assess the effect of truncation in the azimuthal direction, we obtained a complete set of cylindrical near-field data of NSCAT antenna covering 360 degree in ϕ (-180° < ϕ < 1800), and over the full extent of the scanner (3.8 meter long). The data was collected **with the addition of an extra test antenna rotation for each probe position. As an** example, for a given test antenna rotation, the probe samples the field at fixed $\Delta\phi$ for 360 degrees range. During the second test antenna rotation, the probe is free of sampling the field and travels a distance Az. This phenomena is repeated for each probe position, Az, along the scanner. The far-field pattern obtained from the complete near-field scanning in ϕ and the pattern obtained after deleting an interval of near-field data (-30° < ϕ < 30°) corresponding to the back of the antenna is plotted in Fig. 8. It is evident that near-field truncation error in the azimuthal direction will deter our ability to predict the backlobe far-field patterns in that direction. it is seen from Fig. 8 that the pattern deteriorates rapidly in azimuth, starting at an angle (far-field angle) coinciding with the truncated angular near-field region.

E Multiple Reflection Between Probe and Antenna Under Test

The near-field to far-field transformation assumes that multiple reflections between the antenna under and the sampling probe are very small and can be neglected. Since this **is an approximation, we still have to determine how small the reflections are, and its effect on antenna radiation parameters and gain. To accomplish this, a series of** cylindrical near-field measurements which differed in the radial separation by distance of $\lambda/8$ were taken. This procedure was performed to allow correction for multiple reflections. The multipath signals between the probe and the test antenna will have different phase relations at each radial distance r_0 . The relative change in phases is partly due to the change of separation distance and in part due to the multiple reflections. The cylindrical near-field measurement was taken at a radial distance r_0 **=33.6** inch, 33.705 in, 33.810 in, and 33.915 in. The far-fields patterns were computed for each of these near-field measurements. The patterns, H-pol NSCAT antenna 3-D fan beam pattern and contour plot are shown in Figs. 9a and b respectively, were also compared with each other and to the average pattern as illustrated in Fig. 10. It is apparent **that the multiple reflections is in on the order of +/- 0.05 dB over +/- 90° from the peak and will not cause any serious error in the far-field parameters for this antenna and probe pair.** The average antenna pattern and the linear averaging of antenna gain are then used as the correction of the antenna performance. Table 1. shows the NSCAT flight antenna, horizontal polarization, performance parameters obtained from cylindrical near-field measurements on different radial distances. As can be seen in Table 1 that the antenna directivity, defined as the ratio of the maximum radiation intensity (power per unit solid angle) to the average radiation intensity (average over a sphere), varies within 0.004 dB from the linear averaging of directivity of the four measurements. Similar observations have been made for the antenna beamwidth, and pointing in terms of very small variations from the linear averaging value shown in Table 1.

Table 1. NSCAT flight antenna* performance parameters

NSCAT Flight Antenna" H-pol	Antenna Gain (dB)	Antenna Directivity (dB)	Antenna Elevation Beamwidth (Degrees)	Antenna Pointing (Degrees)
r_0=33.600 in	33.488	34.705	0.410	θ=1.829 Φ=0.5
r_0=33.705 in	33.580	34.709	0.409	θ=1.829 Φ=0.5
r_0=33.810 in	33.560	34.704	0.411	θ=1.829 Φ=0.5
r_0=33.915 in	33.551	34.702	0.410	θ=1.829 Φ=0.5
Average	33.545	34.705	0.410	θ=1.829 Φ=0.5

* **NSCAT flight Antenna Serial No.** DPA4/ **H-POL**

G. *Radial Probe Position Error*

Accurate determination of the radial separation distance, r_o, between the center of rotation of the AUT and the phase center of the probe is important to predict antenna gain and relative patterns. **In the near-field to far-field transformation formulation the radial distance r_0 appears in the Hankel function (Appendix A). An evaluation of the sensitivity of the radial measured distance r_0 were performed with computer simulation for different radial errors. Fig. 11 describes the relative change of NSCAT antenna gain from the true pattern (no errors) for different simulated radial errors. A near-field radial error on the order of 0.151 may yield to far-field pattern measurement uncertainty of 0.05** dB **as shown in Fig. 11 over +/- 90 degrees from the peak of the beam.**

H. Probe Scanner Alignment Error

The probe scanner straightness is critical to the determination of the antenna pointing accuracy. In particular, we have found from computer simulation that misalignment of the tower by a tilt angle alpha, causes a pattern shift that is proportional to the slope of the tower. **For an example, a simulation model of** NSCAT **antenna shows that a 0.02**

degrees pointing error in elevation necessitates a probe scanner alignment to better than 1/1 6 of a wavelength. These simulations help in re-fine tuning the scanner. Also, we have measured the probe x,y,z positions, deviation from straight line, for each of its position Az along the scanner. A simulation model of NSCAT antenna is then used to determine the near-field on a cylindrical surface at these probe positions. The far-field is then computed and compared to the pattern obtained with no position errors. It is evident from our simulation analysis that position error magnitude (+/ 0.06 cm) at that level causes no serious errors in the antenna performance parameters.

L Receiver *Drift*

Since the relative long measurement time are required, the receiver system may drift. For an example, NSCAT antenna near-field measurement data acquisition takes little over 6 hours and SeaWinds antenna requires a little over 14 hours. Hence, it is desirable that a correction technique for possible field drift is applied. It is important to note here that the system is very stable during one azimuthal scan but the drift **between the first and the last azimuthal scan can be significant. To correct** for this, normalization scans were taken at the original measurement points. The normalization scans were taken in the vertical direction (z-direction) that is perpendicular to the original scans. This scheme is typically referred to as “tie scan”. For an example, for the case of NSCAT antennas five-normalization scans were taken (at the end of the near-field measurement) in the z direction at a separation distance of $\Delta\phi$=4.0 **degrees. These tie scans were taken over a small area corresponds to the collimated field** region of the antenna, and was used to obtain correction coefficients for all the data set in each linear scan.

4. APPLICATION TO SEAWINDS RADAR ANTENNA

A. SeaWinds Mission Description and Antenna Performance Requirements

Another class of spaceborne scatterometer radar instrument, SeaWinds, has currently been designed at JPL. The instrument is a multi-polarization, multi-incidence angle conical scanning. Fig. 12a shows the SeaWinds conical scan spot-beam illumination. The instrument transmits and receive microwave pulses at ku-band 13.402Ghz to acquire the radar backscattering coefficients over several different azimuth viewing angles. It is designed specifically to measure the winds over 90 % ice free ocean, and it is a follow up on the NSCAT instrument, It will be launched on the Advanced Earth Observation Satellite (ADEOS 11) in 1999 to a polar orbit at approximately 800 km above earth.

The antenna designed for the SeaWinds instrument [22] is a parabolic reflector with an elliptical projected aperture. Fig. 12b shows the flight antenna model. The antenna is built of composite lightweight material (this include the reflector surface shells, **waveguides, struts, and feed-horns) with an rms surface error of 0.2 mm. This antenna** was built by Composite Optics Inc. It is bestowed at an angle of 43 degrees from nadir as illustrated. The projected elliptical aperture of the antenna is 1.07 m X .96 m for the major and minor axis respectively. Two feed horns are placed at +/- 0.0345 meter from the boresight axis of the antenna to produce two independent pencil beams at an angle of 40 and 46 degrees from nadir. The inner beam (beam closer to nadir) is a horizontal polarization, H-pol, with 1.6X 1.8 degrees 3dB beamwidth in elevation and azimuth plane respectively, while the outer beam is a vertical polarization with 1.4 X 1.7 degrees 3dB beamwidth. The inner and outer beam peak gain is designed to be greater than 38.5 dB with cross polarization level for each beam below 20 dB from the peak. The continuous rotation of the reflector antenna, 18 rpm, causes the pencil beam along the spacecraft track to produce a helix scan patterns as shown in Fig. 12a, that each point within the swath width will be viewed by the scan beam two times, once in the forward direction of

the spacecraft, and once in the backward direction. The additional second scan beam will allow the total view of the swath nominally from four different" look' azimuth angles.

B. Seawinds Antenna Calibration

The SeaWinds antenna flight model was measured in the cylindrical near-field range. Because of the feed plate blockage in the center of the scan area, a careful consideration was needed to determine the location, peak of the near-field, at which the normalization point is to be taken. The sampling criteria in ϕ and z of this antenna requires:

$$\Delta\phi \leq 0.8^{\circ}$$
$$\Delta z \leq \lambda/2.$$

Thus, the near-field data density of the SeaWinds antenna is 376 data points in Z (using the full extent of the scanner) by 371 points in ϕ. The total data density, 139,760 points, is more than four times of those needed for **NSCAT antenna. It was necessary that some carefully validation of the measurement and processing technique** for this large amount of data [9]. We had considered two approaches. The first approach was intended for absolute gain calibration, and was carried out with an intercomparison with antenna gain standard measurement performed at the National institute of Standard and Technology (NIST). The second approach was designed for antenna pattern comparative performance with direct far-field measurement.

C. Absolute Gain Verification with Standard Gain Horn

A standard gain horn, SGH, model 12-12 serial No. 193, had been employed to verify the cylindrical near-field measurement set-up and accuracy. This was done by performing an inter-comparison of antenna gain, and patterns using fundamentally different techniques. The horn gain was initially measured at NIST at the SeaWinds frequency, 13.402 **GHz. The measurement was performed using a generalized three-**

antenna measurement technique as described in [21]. Measurement were then performed at JPL using a cylindrical near-field technique to determine the horn patterns and gain. The insertion loss method was used to obtain the horn gain in the cylindrical near-field measurement, and the sampling orthomode probe is used as the gain standard. The cylindrical near-field measurement was carried out at similar measurement parameters that SeaWinds antenna was measured. This included the radial distance, r_0, data density in phi and z (full extent of the scan length in z), frequency, and normalization point. Far-field patterns and antenna gain were then computed from the cylindrical near-field measurement. A comparison between the SGH antenna gain measured at NIST and those measured at JPL in the above described approach shows an excellent agreement (within 0.18 dB) as shown in Table 2. Noteworthy is the fact that different techniques were employed to obtain the antenna gain and yielded results that agreed well.

Table 2. Comparison between standard gain horn antenna measured at NIST using an extrapolation technique and gain measured at JPL using near-field insertion loss **measurement approach.**

JPL SGH Gain Measurement	NIST SGH Gain Measurement	Difference
23.98 dB	23.80 dB	0.18 dB

Furthermore, direct far-field patterns measurement of the SGH were performed at JPL 3000-foot far-field range and compared to those constructed from the cylindrical near-field scanning. Figures 13a, and b show inter-comparison between both measurements for the azimuth and elevation planes respectively. As can be seen, the results are in very good agreement down to 40 dB from the peak of the main beam. It is worthwhile to note here that the 3000-foot far-field range has a limited dynamic range of 40 dB. This is evident in the far-field patterns shown in Fig. 13a at an amplitude level below 40 dB from the peak. Also, it is evident from Figs 13 a, and b that truncation errors start

appearing at an angle greater than +/- 60 degrees in the far-field pattern computed from cylindrical near-field measurement. These results were expected for the SGH that has wide beam patterns and consequently appreciable radiation in the +-/ z direction. Also, this is consistent with the geometrical formula prediction of angular range accuracy in the elevation plane for cylindrical near-field measurement [3], [7]. It is noteworthy to indicate that this inter-comparison of data reported added a factor to the confidence levels in the measurement set-up and procedures, in particular where more than 139,000 near-field data points are measured for the characterization of the SeaWinds radar antenna.

D. Sea Winds Performance Evaluation and Measurement Repeatability

The SeaWinds radar antenna horizontal and vertical polarization were measured in the cylindrical near-field range. Fig. 14 shows the SeaWinds outer beam contour plot far-field pattern as an illustration for the spot beam illumination obtained from cylindrical near-field measurement. The radar antenna performance parameters were then **compared to those obtained in the** JPL's **3000-foot far field range. Figs. 15a and b depict the radiation patterns of the vertical polarization in the elevation and azimuth plane respectively. It is seen that the results are in a very good agreement. Similarly, the horizontal polarization of the SeaWinds antenna was measured and compared to the results obtained in the direct far-field measurement in the elevation and azimuth plane as** shown in Figs. 16a and b respectively.

The SeaWinds antenna was required to a have a fundamental resonant structural frequency of greater than 94 Hz. To meet this requirement, it was necessary to demonstrate the antenna RF performance repeatability pre- and post vibration test. Tables 3 and 4 describe the post-vibration performance parameters obtained from cylindrical near-field measurement for V-pol and H-pol, respectively, and intercomparison with the pre-vibration test results. As can be seen, the relative change of antenna gain is 0.05 dB. The relative change of antenna beamwidth in the elevation

and azimuth planes is within 0.01 degrees. Also, it was noted that antenna pointing in elevation remained the same. Antenna pointing in the azimuth plane varies by 0.1 degrees, and this is due to the mechanical positioner start and stop. Noteworthy, these small changes fall within the measurement uncertainties. Comparison between the pre- and post-vibration test of the antenna principal plane radiation patterns for both the horizontal and vertical polarization shows excellent repeatability [9].

Table 3. SeaWinds outer beam V-pol antenna pre- and post-vibration test performance parameters.

SeaWinds Antenna (V-POL)	Gain (dB)	X-Pol* (dB)	'Beamwidth El (degrees)	Beamwidth AZ (degrees)	Pointing El (degrees)	Pointing Az (degrees)
Requirement	>39.5	**< -20**	1.4 +/-.1	1.7 +/- .1	46 +/- .1	------
Post-vibration test	40.91	-25.63	1,35	1.69	46.08	-0.05
Pre-vibration test	40.86	-25.56	1.34	1.70	46.08	+0.05
Difference	0.05	0.07	0.01	0.01	0.00	0.1

Table 4. SeaWinds inner beam H-pol antenna pre- and post-vibration test performance parameters.

SeaWinds Antenna (H-POL)	Gain (dB)	X-Pol* (dB)	Beamwidth El (degrees)	Beamwidth Az (degrees)	Pointing El (degrees)	Pointing Az (degrees)
Requirement	**>39.2**	**< -20**	1.6 +/- .1	1.8 +/- 0.1	40 +/- .1	------
Post-vibration test	39.27	-26.97	1.66	1.76	40.01	0.00
Pre-vibration test	**39.22**	**-26.54**	**1.66**	**1.76**	**40.02**	+0.10
Difference	0.05	0.42	0.0	0.0	0.01	0.1

"* relative to the peak of the beam

5. CONCLUSION

A cylindrical near-field calibration methodology for spaceborne scatterometer is presented. The methodology demonstrates the utility of cylindrical near-field technique for calibration of large spaceborne Scatterometer antennas by examining various near-field errors and its effect on the far-field patterns. In addition, a generalized technique was introduced to determine the role of probe directivity in cylindrical near-field measurement and the extent and need for introducing probe correction in the calibration of wide beam antenna patterns. The use of standard gain horn for verification of cylindrical near measurement setup was found to be very useful to verify the measurement setup, in particular when large near-field sample data is needed to reconstruct the far-field radiation patterns. Application of cylindrical near-field measurement to the calibration of two recently designed spaceborne scatterometer antennas, NASA **Scatterometer and SeaWinds, together with** our calibration methodology were presented, and demonstrate their successful utility for high precision measurement.

6. APPENDIX

A. Probe Compensation Characterization in Cylindrical Near-Field Scanning

The objective of this appendix is to provide an overview of mathematical steps required to apply probe-compensated near-field measurement technique in a cylindrical configuration. In particular, a novel approach is given in identifying the role of probe pattern compensation.

Consider an idealized circular-aperture probe that is modeled by its equivalent tangential electric currents, $\vec{J}_s$, in the $\hat{x}_p$ = O plane of the probe-coordinate system shown in Fig. 2b. The equivalent currents on the circular-aperture plane maybe modeled as

$$\vec{J}_s = \hat{x}_p \times \vec{H}_p \qquad (1)$$

$$\vec{M}_s = -\hat{x}_p x \vec{E}_p = 0 \qquad (2)$$

Interaction between the probe equivalent aperture currents and the test antenna fields ($\vec{E}_a$, $\vec{H}_a$) can be obtained with the application of reciprocity theorem to yield to the probe vector output (neglecting multiple scattering between the probe and antenna under test)

$$P^{(1,2)} = \int_{S_{11}} \left(\vec{M}_s \cdot \vec{H}_a - \vec{J}_s \cdot \vec{E}_a \right) ds \qquad (3)$$

In equation (3), superscripts (1 ,2) designate two orientations of the probe necessary to construct the far-field pattern of the test antenna. Specifically, P^1 and P^2 correspond to the probe response for the electric current, $\vec{J}_s$, oriented in the $\hat{z}_p$ and $-\hat{y}_p$ direction respectively. Assuming a uniform current across the probe, the integral in equation (3) is then approximated by

$$P^1 \approx \int_{S_p} E_z(\rho,\phi,z)\rho_p d\phi_p d\rho_p \tag{4}$$

$$P^2 \approx \int_{S_p} E_\phi(\rho,\phi,z)\rho_p d\phi_p d\rho_p \tag{5}$$

where (ρ_p, ϕ_p) defines the polar coordinate in the aperture of the probe S_p, and E_z, E_ϕ are the fields in the cylindrical-coordinate system of the test antenna computed on the probe **aperture. The use of an idealized circular-aperture probe with different radii, permits us to** derive a closed form expression for its far-field radiation pattern. For a uniform magnetic field, *H,* in the aperture of the probe oriented in the y_p direction, the probe pattern can be written as

$$\vec{E}^1_{\theta_p} = \sin\theta_p \frac{J_1(u)}{u}\hat{\theta}_p \tag{6}$$

$$\vec{E}^1_{\theta_p} = 0\hat{\phi}_p \tag{7}$$

and for a 90°" rotation of the probe, it yields

$$\vec{E}^2_{\theta_p} = \cos\theta_p \sin\phi_p \frac{J_1(u)}{u}\hat{0}_1, \tag{8}$$

$$\vec{E}^2_{\phi_p} = \cos\phi_p \frac{J_1(u)}{u}\hat{\phi}_p \tag{9}$$

where $u=ka\sin(\alpha), \cos(\alpha)=\sin(\theta_p)\cos(\phi_p)$, *a is* the probe radius, *k* is the wavenumber $2\pi/\lambda$, and $J_1(u)$ is the Bessel function of the first kind. To perform probe-pattern compensation, one needs the cylindrical wave expansion of the probe fields from the following expressions (assuming no fields in the back of the probe):

$$a_m^2\left(k\cos\theta_p\right) = \frac{1}{j^m \sin\theta_p} \int_{-\pi/2}^{\pi/2} E_{\phi p}^2\left(\theta_p, \phi_p\right) e^{-jm\phi_p} d\phi_p \qquad (10)$$

$$b_m^2\left(k\cos\theta_p\right) = \frac{1}{j^{m+1} \sin\theta_p} \int_{-\pi/2}^{\pi/2} E_{\theta p}^2\left(\theta_p, \phi_p\right) e^{-jm\phi_p} d\phi_p \qquad (11)$$

where $m < ka$. Similarly, one could obtain the probe coefficients, a^1_m and b^1_m, for the other field components, $E^1_{\theta p}$ and $E^1_{\phi p}$. These results, together with the probe vector output response (equations 4–1 1 are numerically evaluated) allow us to perform computer-simulated synthetic measurements and provide accurate insight unattainable or costly in measurement alone. The test antenna fields, E_θ and E_ϕ, are then constructed in terms of the probe vector output response and probe antenna coefficients derived from application of the reciprocity theorem to obtain

$$\vec{E}_\phi(\theta,\phi) = \sin\theta \sum_{|n|<kr} j^n a_n\left(k\cos\theta\right) e^{jn\phi}\hat{\theta} \qquad (12)$$

$$\vec{E}_\theta(\theta,\phi) = \sin\theta \sum_{|n|<kr} j^{n+1} b_n\left(k\cos\theta\right) e^{jn\phi}\hat{\phi} \qquad (13)$$

where r is the smallest radius enclosing the test antenna and a_n, b_n are the cylindrical wave coefficients of the test antenna and given by

$$a_n\left(k\cos\theta\right) = \frac{T_n}{\sin^2\theta\,\Delta_n\left(k\cos\theta\right)} \left[\left(k\cos\theta\right)\alpha_m^2\left(k\cos\theta\right) - T_n^2\left(k\cos\theta\right)\alpha_m^1\left(k\cos\theta\right)\right] \qquad (14)$$

$$b_n\left(k\cos\theta\right) = \frac{T_n}{\sin^2\theta\,\Delta_n\left(k\cos\theta\right)} \left[T_n^2\left(k\cos\theta\right)\gamma_m^2\left(k\cos\theta\right) - T_n^1\left(k\cos\theta\right)\gamma_m^2\left(k\cos\theta\right)\right] \qquad (15)$$

$$T_n^{(1,2)}(k\cos\theta) = \int_{-\infty}^{\infty}\int_{-\pi}^{\pi} P^{(1,2)} e^{-jn\phi} e^{jk\cos\theta z}\, d\phi dz \qquad (16)$$

in which $P^{(1,2)}$ is the near-field measured data or simulated data for the two different orientations of the probe. The integration in z is truncated to extend over the measured scan distance ($Z_{min} < z < Z_{max}$) and

$$\Delta_n(k\cos\theta) = \gamma_m^1(k\cos\theta)\alpha_m^2(k\cos\theta) - \gamma_m^2(k\cos\theta)\alpha_m^1(k\cos\theta) \qquad (17)$$

$$\alpha_m^{(1,2)}(k\cos\theta) = \sum_{|m|<ka} b_m^{(1,2)}(k\cos\theta_p)\, H_{n+m}^2(k\, r_0 \sin\theta) \qquad (18)$$

$$\gamma_m^{(1,2)}(k\cos\theta) = \sum_{|m|<ka} a_m^{(1,2)}(k\cos\theta_p)\, H_{n+m}^2(k\, r_0 \sin\theta) \qquad (19)$$

where H^2_{n+m} is the Hankel function of the second kind and r_0 is the sampling cylinder radius. The Fourier integral **in equation 16 can be evaluated with the application of two dimensional FFT over the measured data in ϕ and z. However, in** our implementation of the algorithm for the computation of the test antenna patterns, we perform a numerical integration in Z and one dimensional FFT in ϕ on equation 16. This approach yields to specify the elevation and azimuth angles observation points at which the far field is desired to be calculated [7]. In addition, this implementation facilitates efficient computation of the near-field on planar surfaces for microwave imaging and holographic diagnostic of test antennas [23]. Noteworthy, this is done without resorting to interpolation among far-field observation points.

In the limit as the probe radius becomes very small, the probe output of equation 3 is the direct response of the near field at a point, that is the response of infinitesimal hertzian dipole, $P^1 = E_z$ and $P^2 = E_\phi$, and no probe compensation is needed. Also, note from equations 10 and 11 and Fig. 2 that probe compensation at observation angle O

necessitates the knowledge of the probe fields in the azimuthal direction at observation angle $\theta_p=\pi-\theta$. Consequently, the calculation of the principal elevation plane of the test antenna, for example, requires the knowledge of three dimensional radiation probe far-field patterns. Hence, a priori to near-field measurement, the sampling probe far-field patterns must be known.

Two different test antenna simulation examples are considered: 15-element infinitesimal dipole array, and the JPL/NASA scatterometer (NSCAT) slotted-waveguide radar antenna. The first model is very attractive for implementation since closed form expressions for the far-field is readily available, and it posses a circular symmetry that near-field probe response need only to be computed along single z-scan. The complete near-field data set can then be extracted from this data. The 15-element array model results are presented in [15] and are not addressed here. The result of NSCAT antenna is presented in subsection 3B and Fig. 6.

REFERENCES

[1] F.M Naderi, M.H Freilich, and D.G Long, " Spaceborne radar measurement of wind velocity over the ocean- An overview of the NSCAT scatterometer system" Proc. of the IEEE, vol. 79, No. 6, pp 850-866, June 1991.

[2] A.D. Yaghjian, " An Overview of Near-Field Antenna Measurements," *IEEE Trans. Antennas and Propagat.,* vol. Ap-34, No. 1, pp 30-45, Jan. 1986.

[3] Special Issue On Near-Field Scanning Techniques, *IEEE Trans. Antennas and Propagat.*, *vol. Ap-36,* June 1988.

[4] W.M. Leach Jr. and D.T Paris, "Probe compensated near-field measurements on a cylinder," *IEEE Tran.* Antennas *and Propagat.,* vol. AP-21, No 4, pp. 435-445, July 1973.

[5] A.D. Yaghjian, **"Near-field antenna measurement on a cylindrical surface: A source** scattering-matrix formulation," NBS Tech. Note 696, Sept. 1977.

[6] G.V. Borgiotti, " Integral equation formulation for probe corrected far-field reconstruction from measurements on a cylinder" IEEE Trans. Antennas Propagat., vol. AP-26, pp 572-578, July 1978

[7] Z.A. Hussein, " Efficient and fast reconstruction of the far-field radiation pattern from knowledge of the near-field on a cylindrical surface" Tech Rept., JPL, California institute of Technology,-Vetlt+m&tle, 43-91 24; Nov 8, 1991 ~ JPL Internal Rept. no. D-91 3-y, Nov. 8, 1991.

[8] Z. A. Hussein and Y. Rahmat-Samii "Probe compensation characterization in cylindrical near-field scanning" 1993 IEEE Antennas Propagat. Sot, International Symp., Ann Arbor, Michigan, June 1993.

[9] Z.A. Hussein, and Y. Rahmat Samii, " On the accurate calibration of the SeaWinds radar antenna: A cylindrical near-field measurement approach" 1996 International Geoscience And Remote Sensing Symposium, 96' IGARSS, Digest, Lincoln, Nebraska, May 1996.

[1 O] Z. A. Hussein and Y. Rahmat-Samii "Cylindrical near-field measurement error model for NASA Scatterometer fan- beam array antenna" 1992 IEEE Antennas Propagat.Sot, International Symp., Chicago, Illinois.

[11] A.C. **Newell,** "Error Analysis Technique for Planar Near-Field Measurements," *IEEE Trans., Antenna and Propagat.*, **Vol.** AP-36, pp. 754-768, June 1988.

[12] A.C. Newell and C. F. Stubenrauch "Effect of random errors **in planar near-field measurement"** */EEE Trans., Antenna and Propagat.*, **Vol.** AP-36, **pp. 769-773, June 1988.**

[13] A.D. Yaghjian, "Upper-bound errors **in far-field antenna parameters determined from planar near-field measurements, Part 1: Analysis," National Bureau of Standard and Technology. Note 667,1975.**

[14] **A. C. Newell, " Upper-bound errors in far-field antenna parameters determined from planar near-field measurements, Part 2: Analysis and computer** simulation,," **National Bureau of Standard and Technology. lecture notes for National Bureau of Standard and Technology, July 1975.**

[15] Z. A. Hussein "Probe Compensation And Error Analysis In Cylindrical Near-Field Scanning" *16th annual Antenna and Measurement Techniques Symp., AMTA, Symposium,* Digest, Long Beach California, October 1994.

[16] Y. Rahmat-Samii, L. Williams, R.G. Yaccarino, **"The UCLA hi-polar planar** near-**field measurement and diagnostics range" IEEE Antenna and Propagation Magazine, vol. 37,** No. **6, Dec. 1995, pp 16-35**

[17] J. J. H. Wang " An examination of the theory and practices of planar near-field measurement", */EEE Trans. Antennas and Propag., vol. 36, No 6,* June 1988, pp 746-753.

[18] Y. Rahmat-Samii, V. Galindo and R. Mittra, "A plane-polar approach for far-field construction from near-field measurements", *IEEE Trans. Antennas and Propagation,* vol. AP-28, pp. *216-230,* March 1980.

[19] L.1. Williams, Y. Rahmat-Samii, and R.G. Yaccarino, "The hi-polar planar near-field measurement technique, part 1: implementation and measurement comparisons," *IEEE Trans. Antennas Propagat.*, vol. AP-42, pp. 184-195, February 1994.

[20] J.E. **Hansen, "Spherical Near-Field Antenna Measurements" Published by Peter Peregrinus** Ltd, London, UK, 1988.

[21] A. C. Newell, R.C. Baird, and P.F. Waker, "Accurate measurement of antenna gain and polarization at reduced distances by an extrapolation technique," *IEEE Trans Antenna Propagat., vol.* Ap-21,No *4,* pp 418-431, July 1973

[22] Z. A. Hussein, Y. Rahmat-Samii, **and K. Kellogg, "Design And Near-Field Measurement Performance Evaluation of The SeaWinds Dual-Beam Reflector Antenna" 1997 IEEE Antennas And Propagation International Symposium and URSI North American Radio** Science Meeting, Montreal, Canada.

[23] Z. A. Hussein “Microwave imaging and holographic diagnostic to antennas in cylindrical near-field scanning” 1995 IEEE AP-S/Union Radio Science International Symposium, URSI Digest, NewPort Beach, California, June 1995.

ACKNOWLEDGEMENT

This work was carried out at the Jet Propulsion Laboratory, California Institute of Technology, under contract with the National Aeronautics and Space Administration. The authors would like to thank Mrs R. Thomas, C. Chavez, for their assistance in the measurements, and Mr K. Kellogg and the NASA Scatterometer/SeaWinds project office for supporting this work. The authors also thank Drs. E. Im, T. Freeman, and J. Van Zyl for their support to complete this work.

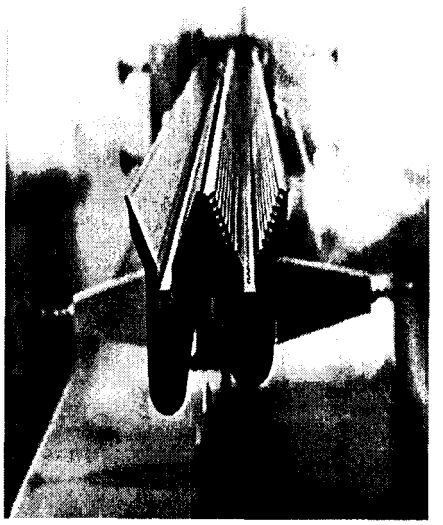

Figure 1. Dual-polarization (H-pol and V-pol) Ku-Band NASA Scatterometer (NSCAT) flight antenna.

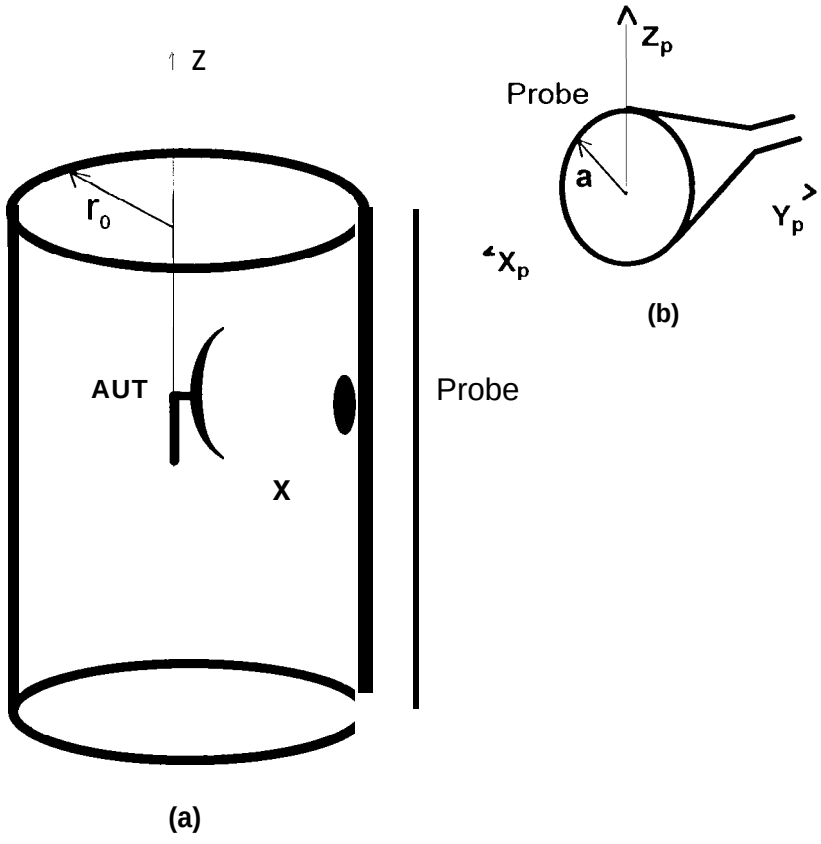

Figure 2. (a) Cylindrical near-field measurement geometry. (b) Probe coordinate system

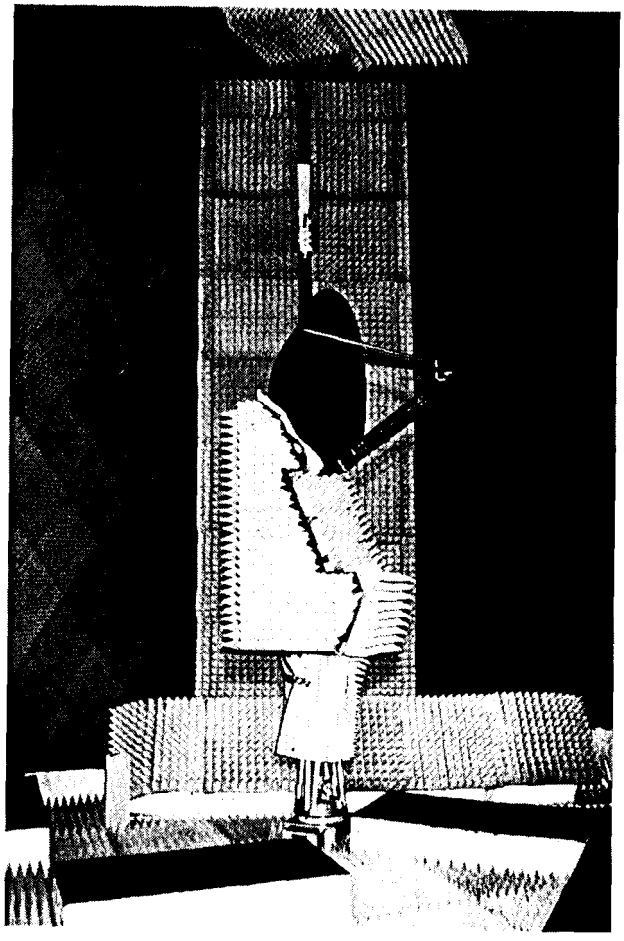

Figure 3. SeaWinds dual-beam reflector antenna mounted in the cylindrical near-field measurement facility at JPL. In the front, the antenna is placed on a horizontally rotating positioner. In the back, the probe is linearly translated along a vertical track.

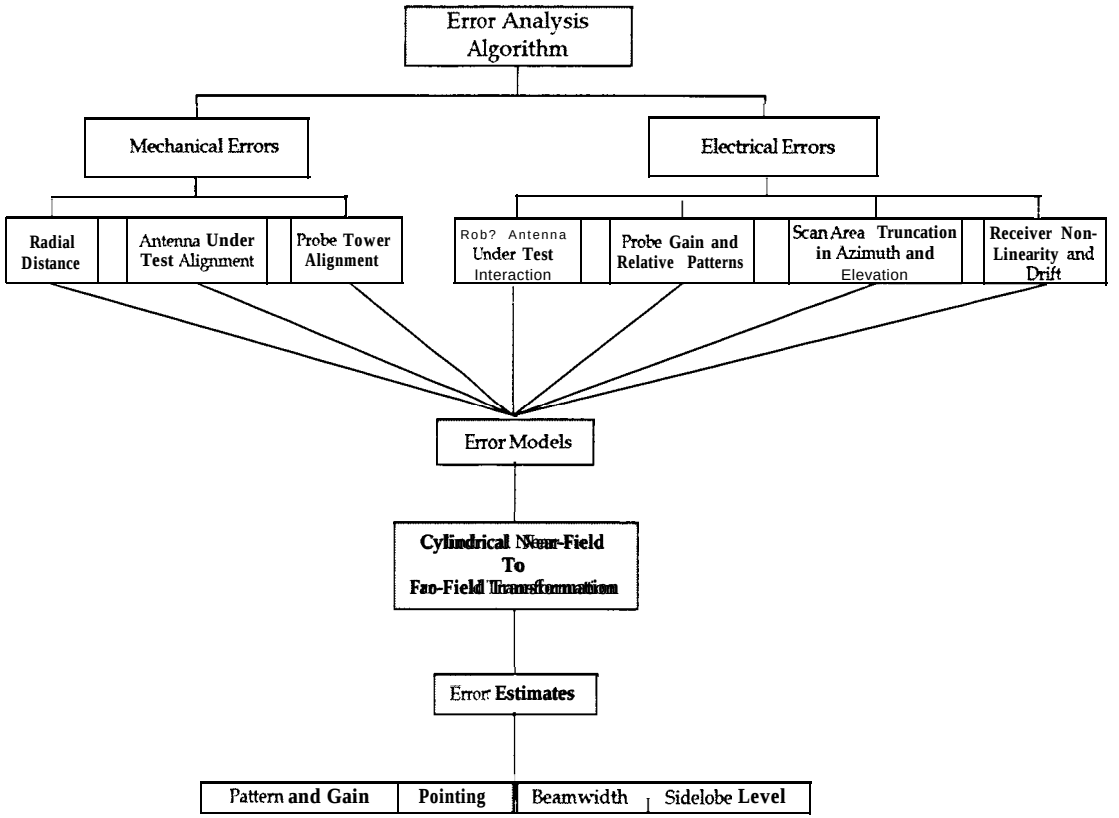

Figure 4. Cylindrical near-field error analysis algorithm

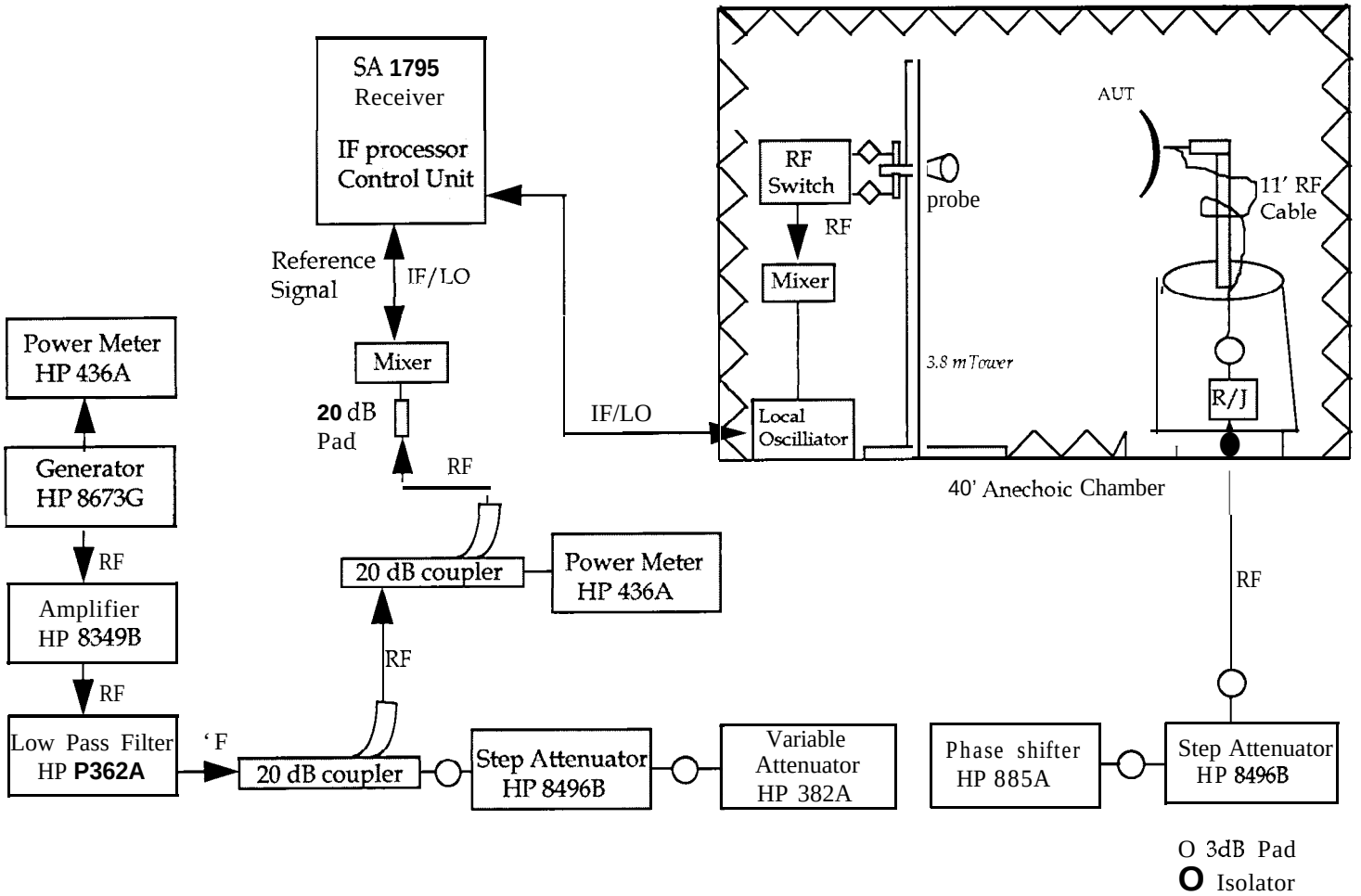

Figure 5. JPL cylindrical near-field range measurement setup

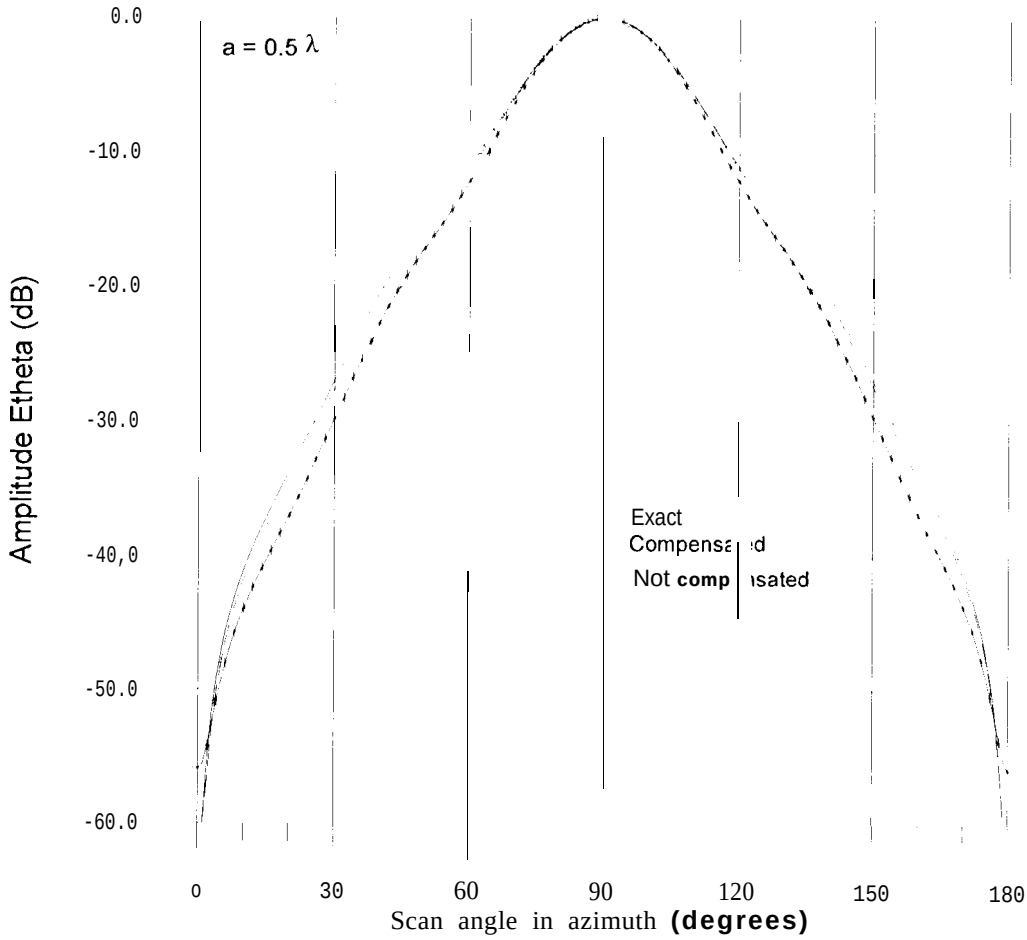

Figure 6. Comparison of exact solution and NSCAT far-fields obtained from simulated near-field with and without probe pattern compensation. The need of probe correction can be observed starting at an angle of 20 degrees from the peak of the beam, The probe radius , a, used in the simulation is 0.5λ.

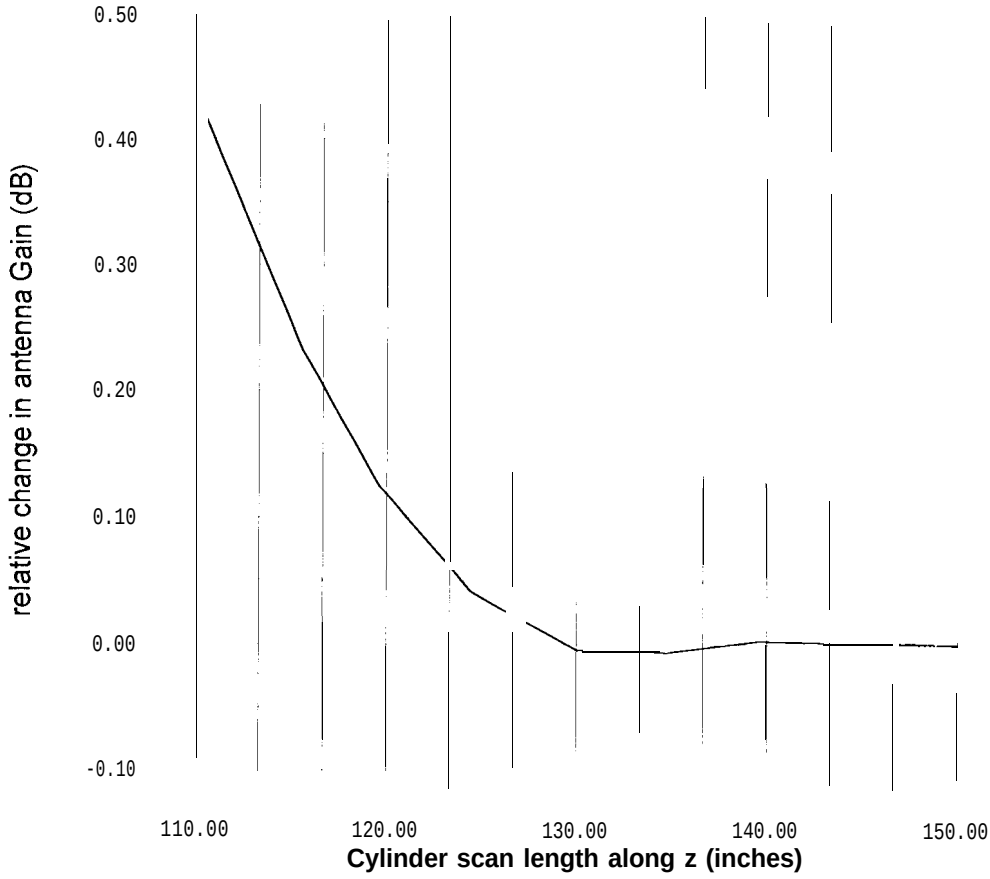

Figure 7. Relative change in NSCAT antenna measured gain Vs truncated cylinder length in z-direction

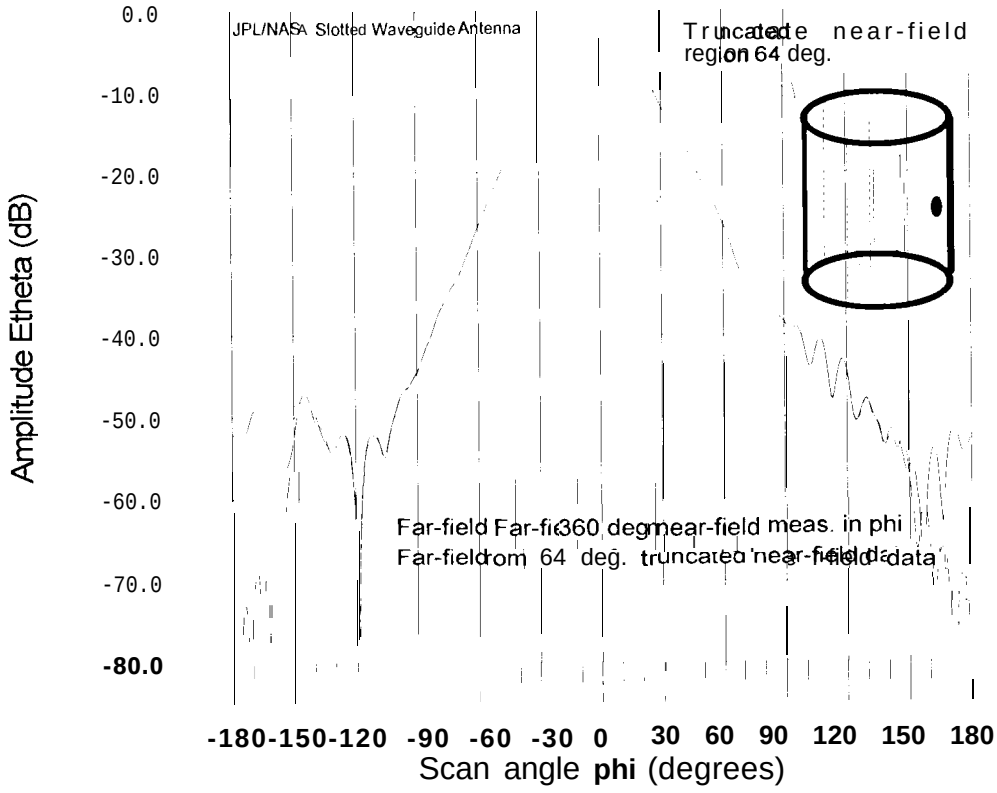

Figure 8. Comparison of NSCAT antenna far-field radiation patterns constructed from complete near-field measurement in azimuth (360 degrees) and truncated interval (60. degrees)

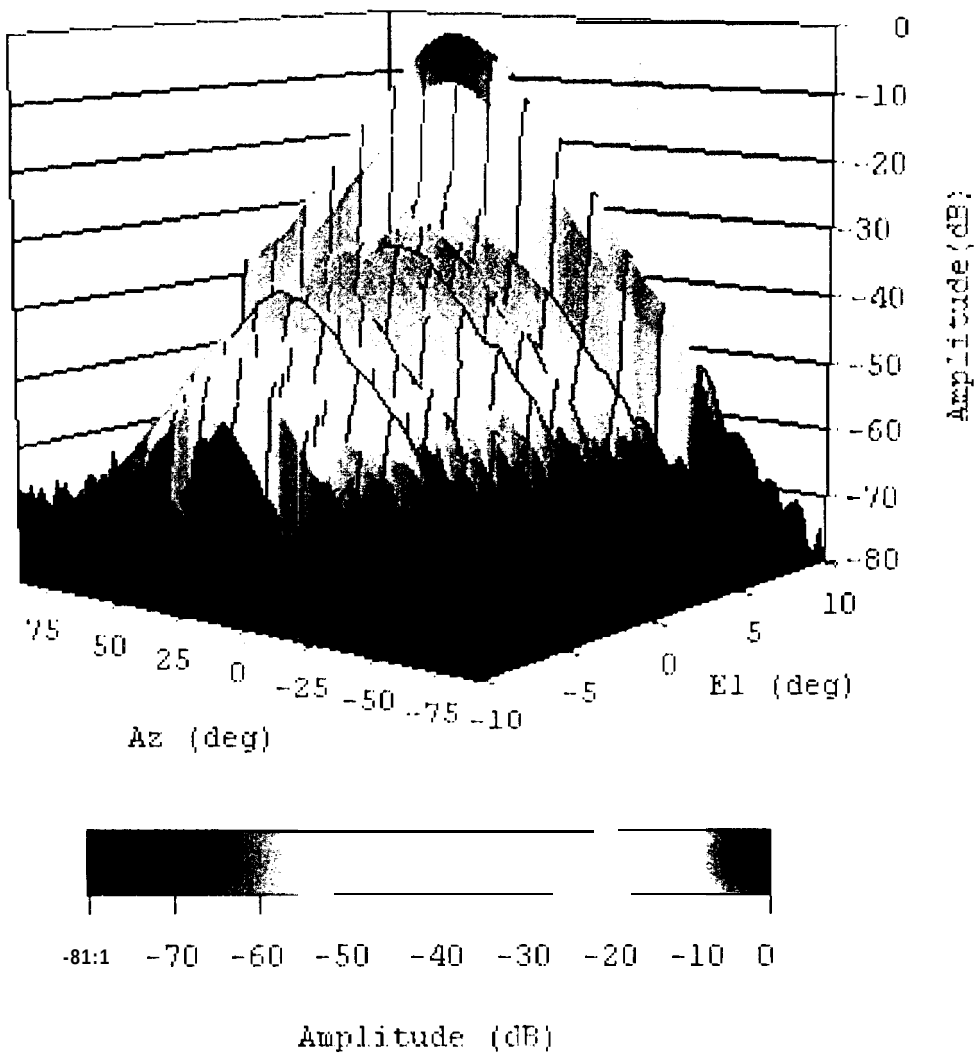

Figure 9a. NSCAT H-pol far-field radiation pattern obtained from cylindrical near-field measurement taken at r_o = 33.6 in.

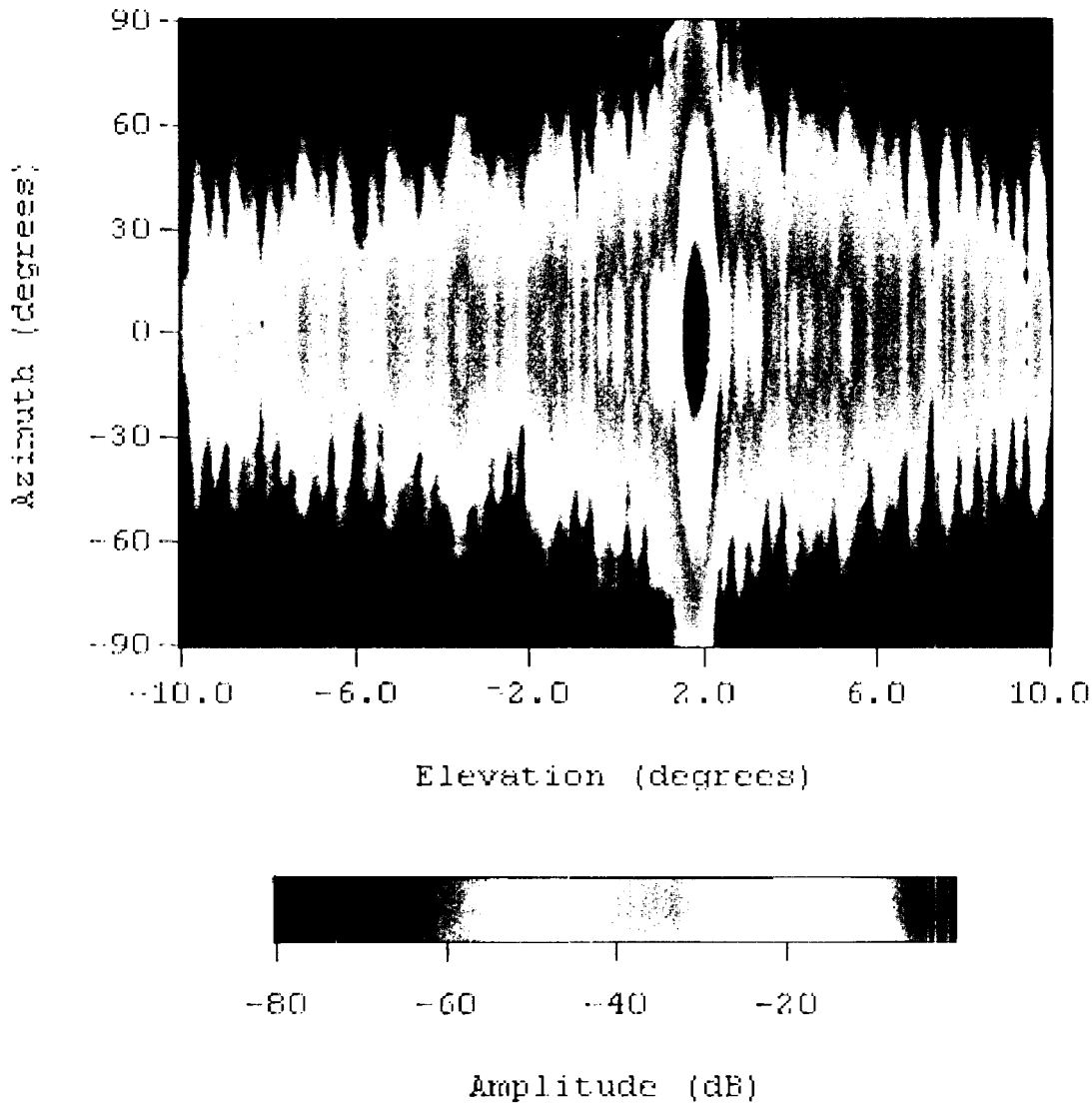

Figure 9b. NSCAT antenna far-field pattern (fan-beam) contour plot obtained from cylindrical near-field measurement.

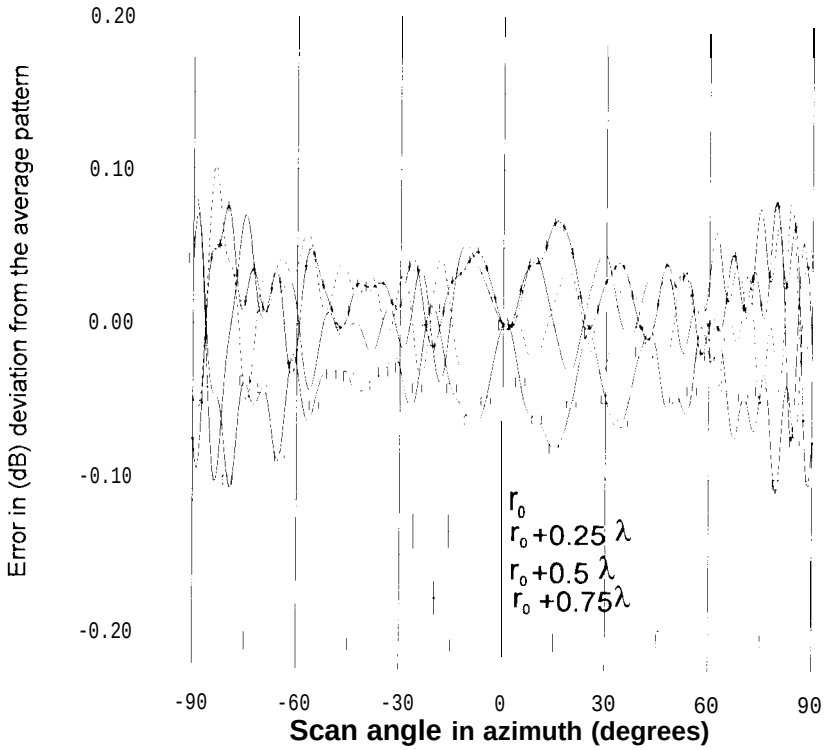

Figure 10. Error estimate (based on measured data) on the far-field radiation pattern clue to near-field multiple reflection between probe and NSCAT antenna,

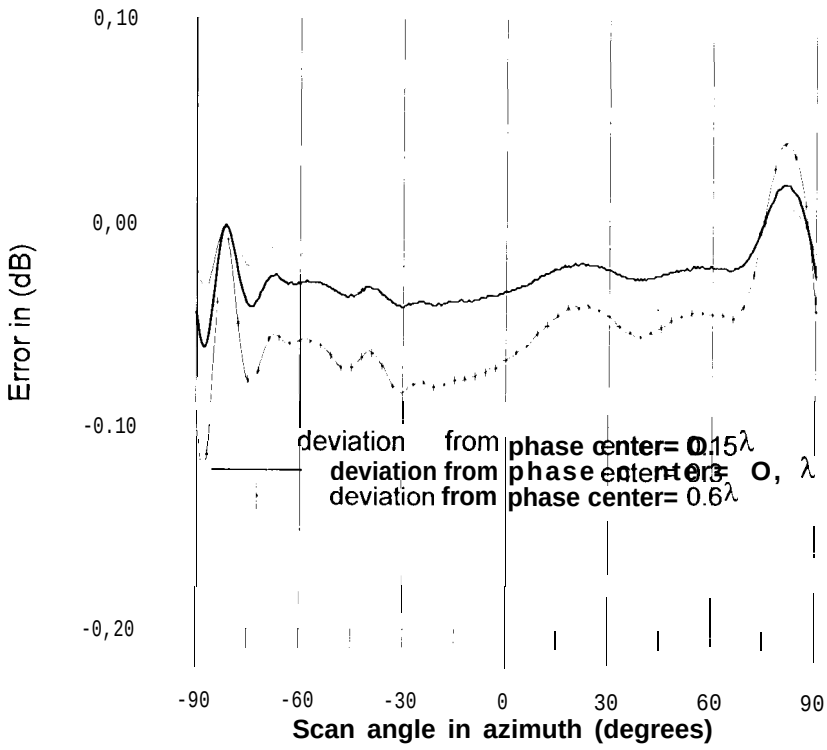

Figure 11. Error estimate on NSCAT far-field patterns due to near-field radial distance measurement errors Vs. scan angle in azimuth direction

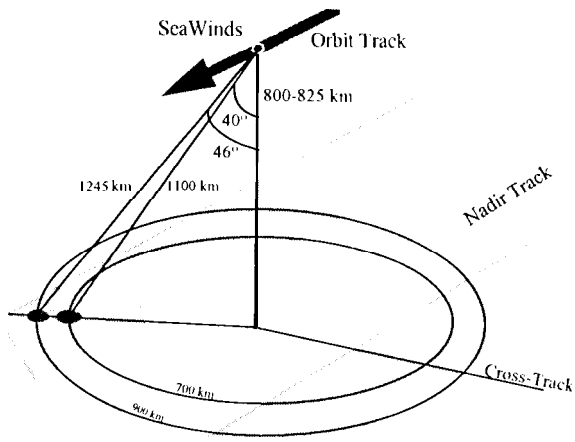

(a)

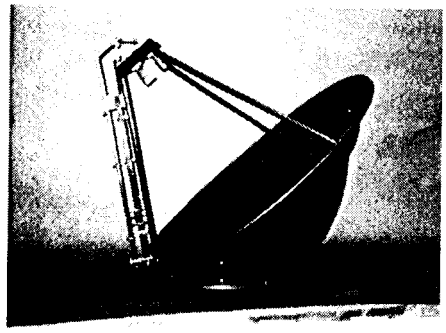

(b)

Figure 12. (a) SeaWinds conical-scan spot-beam illumination, (b) SeaWinds dual-feed flight reflector antenna. The antenna shell, waveguides, feed-horn, and feed support plate are all made of lightweight composite material (total weight is 6.4 kg).

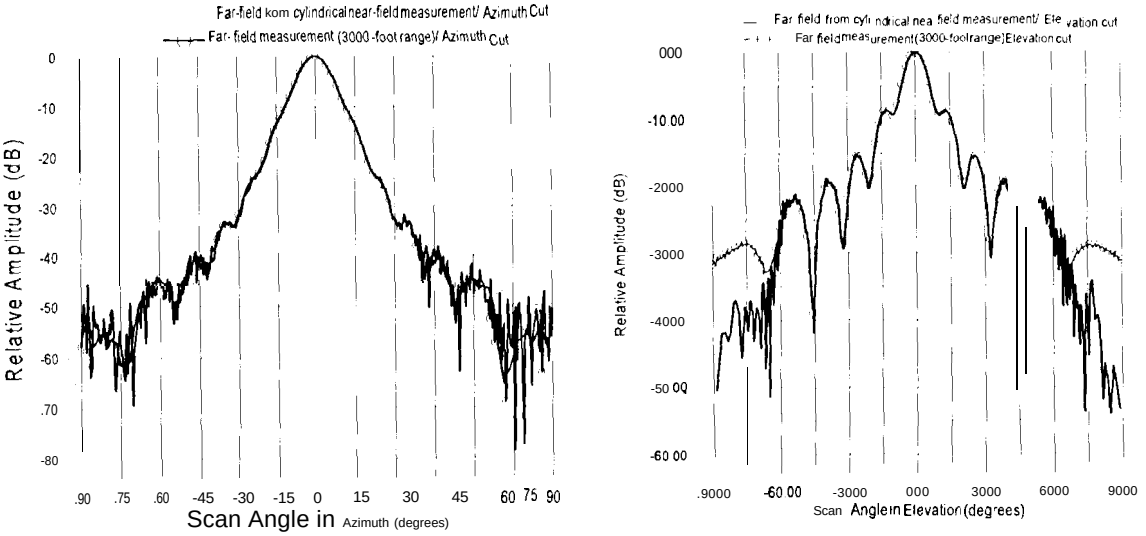

(a) (b)

Figure 13. Comparison of standard gain horn far-field radiation pattern obtained from cylindrical near-field measurement and direct far-field measurement. (a) azimuth plane (b) elevation plane

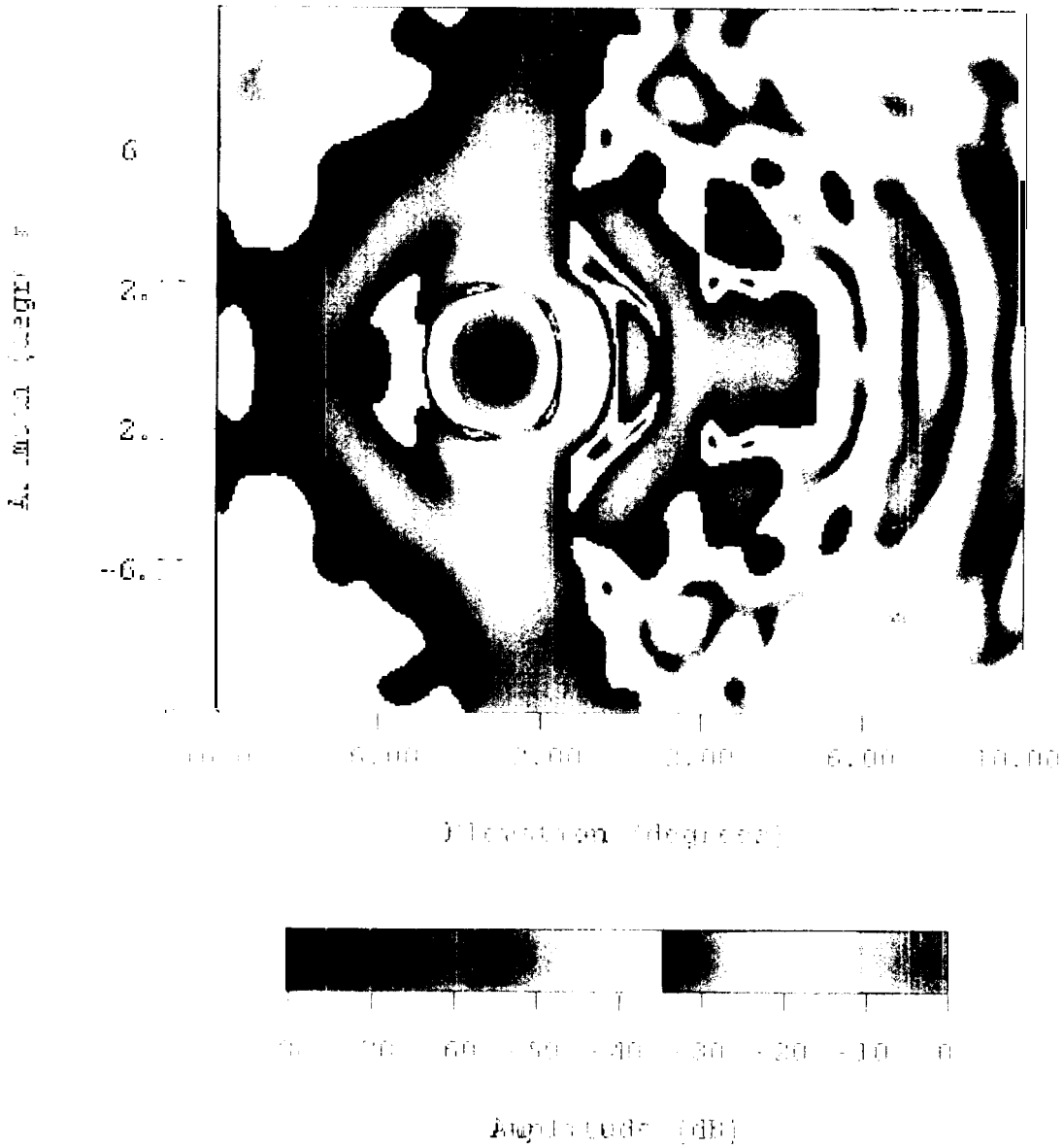

Figure 14. Spherical far field pattern (circular beam) contour plot obtained from cylindrical near field measurement.

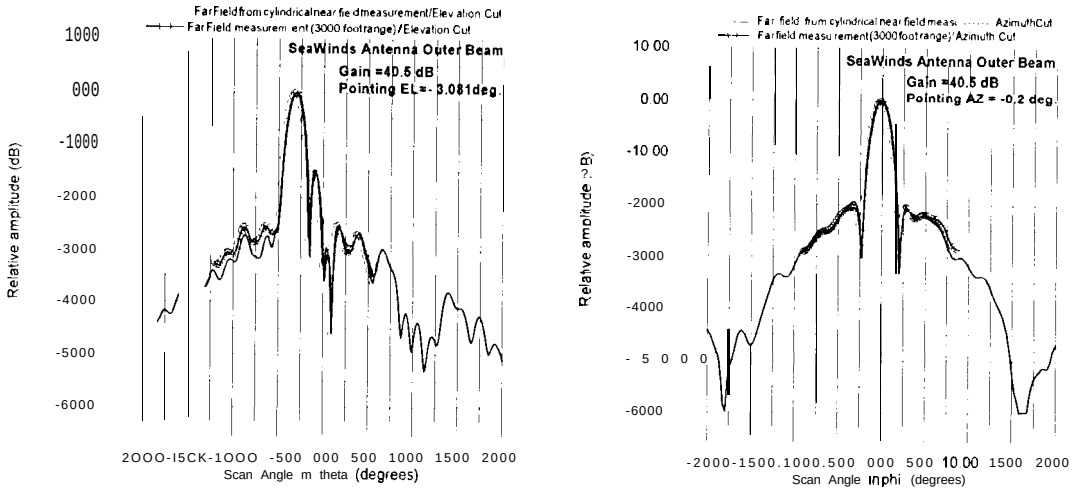

(a) (b)

Figure 15. Comparison of outer beam V-pol SeaWinds radar antenna far-field pattern obtained from cylindrical near-field measurement and direct far-field measurement. (a) elevation plane, (b) azimuth plane.

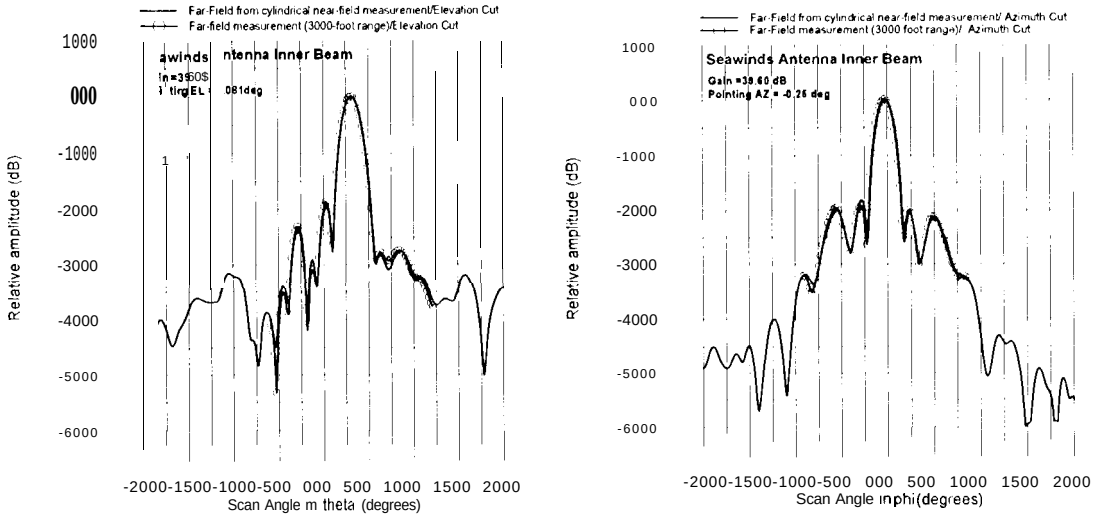

(a) (b)

Figure 16. Comparison of inner beam H-pol SeaWinds radar antenna far-field pattern obtained from cylindrical near-field measurement and direct far-field measurement. (a) elevation plane, (b) azimuth plane.

Ziad A. Hussein was born in Beirut, Lebanon, and is currently pursuing the Ph.D degree in Electrical Engineering at the University of California, Los Angeles (UCLA). He received his M.S degree in Electrical Engineering in 1991, where his M.S. thesis was on the method of moment analysis of quadrifilar helix antenna radiation characteristics and phase center stability for Global Positioning System (GPS) applications, and the B.S. degree from the University of Massachusetts at Amherst in Electrical Engineering.

He joined the Jet Propulsion Laboratory, California Institute of Technology, Pasadena in 1991, where he is a member of the technical staff in the Radar Science and Engineering Section. He has made fundamental contribution to the design, analysis and near-field calibration of the SeaWinds Spaceborne Scatterometer instrument (he is currently the Cognizant Engineer for the SeaWinds radar antenna and the Cognizant Engineer for near-field radar antenna calibration). He led the near-field error analysis algorithm development, cylindrical near-field calibration, and RF performance characterization of all NASA Scatterometer (NSCAT) flight and spare antennas. He recently proposed the X-band design configuration and designed the X-band offset reflector antenna for the LightSAR preproject.

Mr. Hussein is a member of the IEEE Antennas and Propagation Society (AP-S), and the IEEE Geoscience and Remote Sensing Society. He was on the Technical Organization Committee and a Session Chairman of the 1995 IEEE AP-S/Union of Radio Science Joint International Symposium. He was also on the organization Committee of the Antenna Measurement Techniques Association (AMTA), which hosted the 1994 AMTA International Symposium. He has also reviewed papers for both the Journal of Electromagnetic Waves and the IEEE Transactions on Antennas And Propagation. In 1997, he received NASA Group Achievement Award, and file two new technology reports by 1996.

Mr. Hussein's research interest is in applied electromagnetic, subsurface remote sensing, Synthetic Aperture Radar (SAR) interferometery and polarimetry, antennas and advance near-field calibration techniques.

Yahya Rahmat-Samii is a Professor of Electrical Engineering at the University of California, Los Angeles (UCLA). Before joining UCLA, he was a Senior Research Scientist at Jet Propulsion Laboratory, California Institute of Technology. He receiver! his M.S. and Ph.D. degrees in Electrical Engineering from the University of Illinois, Champaign-Urbana.

Dr. Rahmat-Samii was the elected 199S President of IEEE Antennas and Propagation Society and was appointed an IEEE Distinguished Lecturer and presented lectures internationally. He was elected as a Fellow of the IEEE in 1985 and a Fellow of the IAE in 1986. He was also the 1984 recipient of the prestigious Henry Booker Award of USNC/URSI. He has authored and co-authored over 380 technical journal art icles and conference papers and has written 14 book chapters and a book entitled, Impedance Boundary Conditions in Electromagnetics. He is also the holder of several patents. His research contributions cover a diverse area of electromagnetic, antennas, satellite and personal communications **(visit http: //www.antlab.ee.ucla.edu).**

For his contributions, Dr. Rahmat-Samii has received numerous NASA/JPL awards, In 1992 and 1995, he was the recipient of the Best Application Paper Award (Wheeler Award) for papers published in the 1991 and 1993 IEEE AP-S Transactions. In 1993, 94 and 95, three of his Ph.D. students were named the Most Outstanding Ph.D. Students at UCLA's School of Engineering and Applied Science and another received the Best Student Paper Award at the 1993 IEEE AP-S Symposium. He is a member of Commissions A, B and J of USNC/URSI, AMTA, Sigma Xi, Eta Kappa Nu and the Electromagnetic Academy and is listed in Who's Who in America, Who's Who in Frontiers of Science and Technology and Who's Who in Engineering.